Tech Science Press

Cardioprotective effect of ivabradine via the AMPK/SIRT1/PGC-1α signaling pathway in myocardial ischemia/reperfusion injury induced in H9c2 cell

Xingxing Zhu[1,2]; Tianfeng Hua[1,2]; Mingfei Wu[3]; Jiatian Wu[1,2]; Jianchao Hong[1,2]; Min Yang[1,2,*]

[1] The Second Affiliated Hospital of Anhui Medical University, Hefei, China
[2] The Laboratory of Cardiopulmonary Resuscitation and Critical Care Medicine, The Second Affiliated Hospital of Anhui Medical University, Hefei, China
[3] School of Pharmacy, Anhui Province Key Laboratory of Major Autoimmune Diseases, Anhui Medical University, Hefei, China

Abstract: Post-resuscitation myocardial dysfunction (PRMD) is the most severe myocardial ischemia-reperfusion injury (MIRI) and is characterized by difficult treatment and poor prognosis. Research has shown the protective effects of the rational use of ivabradine (IVA) against PRMD; however, the molecular mechanisms of IVA remain unknown. In this study, an ischemia-reperfusion injury (IRI) model was established using hypoxic chambers. The results demonstrated that pretreatment with IVA reduced IRI-induced cytotoxicity and apoptosis. IVA attenuated mitochondrial damage, eliminated excess reactive oxygen species (ROS), suppressed IRI-induced ATP and NAD$^+$, and increased the AMP/ATP ratio. We further found that IVA increased the mRNA levels of sirtuin 1 (*SIRT1*) and peroxisome proliferator-activated receptor-γ coactivator 1α (*PGC-1α*) and upregulated the expression levels of phosphorylated AMP-activated protein kinase (p-AMPK)/AMPK, SIRT1, and PGC-1α proteins. Interestingly, no change in AMPK mRNA levels was observed. Cardiomyocyte energy metabolism significantly changed after IRI. The aim of this study was to demonstrate the cardioprotective effect of Ivabradine via the AMPK/SIRT1/PGC-1α signaling pathway in myocardial ischemia/reperfusion injury-induced in H9c2 cell.

Introduction

Post-resuscitation myocardial dysfunction (PRMD) is the most severe myocardial ischemia-reperfusion injury (MIRI) and is closely associated with early death after resuscitation, especially within the first 24 h after the restoration of spontaneous circulation (ROSC) (Jentzer *et al.*, 2015). Studies have shown that the severity of PRMD is closely related to the duration of myocardial ischemia and the dose of epinephrine (Palmer *et al.*, 2004; Yamaguchi *et al.*, 2002). In the resuscitation process of cardiac arrest (CA) patients, the use of epinephrine (especially large doses) can significantly increase the heart rate after resuscitation and the recurrence rate of arrhythmia, and even ventricular fibrillation after resuscitation and those factors would aggravate PRMD. Therefore, controlling the heart rate is one of the clinical methods used to treat cardiovascular diseases (Yip *et al.*, 2016). Many previous studies have reported the therapeutic

value of β-blockers for PRMD in animal models and clinical studies (Zhang and Li, 2013; Ji *et al.*, 2012; Link *et al.*, 2015; Yang *et al.*, 2015). The limited use of beta-blockers to treat PRMD patients is probably due to their negative inotropic, negative chronotropic, and negative dromotropic effects (Link *et al.*, 2015). Therefore, it is necessary to find new safe and effective drugs for controlling heart rate.

IVA is the only hyperpolarization-activated cyclic nucleotide-gated (HCN) channel inhibitor that has been demonstrated to control heart rate and protect heart function to date (Kuwabara *et al.*, 2013; Xia *et al.*, 2010; Yu *et al.*, 2015). In fact, the IVA treatment was compared with the effect of beta-blockers. Evidence provides that IVA treatment is associated with an increase in the ejection fraction (EF) and reductions in end-diastolic volumes (EDVs) and end-systolic volumes (ESV)s (Fasullo *et al.*, 2009). Our previous results also indicated that IVA could alleviate myocardial dysfunction and myocardial injury in a porcine cardiopulmonary resuscitation (CPR) model, suggesting that IVA may be beneficial for the treatment of PRMD patients (Yang *et al.*, 2020).

In clinical practice, patients with acute coronary syndrome (ACS) have got beneficial effects with the administration of IVA (Oliphant et al., 2016; Trivi et al., 2014). A further study found that IVA has multi-effects such as anti-inflammatory, antioxidant, and endothelial cell function improvements (Li et al., 2013; Marazia et al., 2015; Custodis et al., 2008). Furthermore, IVA could reduce myocardial oxygen consumption, without affecting myocardial contraction or inducing heart arrhythmias (Treptau et al., 2015). Under heart rate control conditions, IVA protects against MIRI primarily by reducing the range of myocardial infarction and the production of reactive oxygen species (ROS), and by increasing the activity of ventricular myocytes and adenosine triphosphate (ATP) in mitochondria (Kleinbongard et al., 2015). However, the molecular mechanism underlying these protective effects of IVA remains unknown.

The MIRI effect may be controlled by decreasing ATP production and oxidative stress levels, avoiding the increase of apoptosis (Yellon and Hausenloy, 2007; Ovize et al., 2010). This study investigated the cytoprotective effects of IVA against ischemia-anoxia-induced heart injury, especially the role of AMP-activated protein kinase (AMPK). AMPK is a well-known intracellular energy receptor that protects against metabolic stress conditions, such as ischemia/reperfusion (I/R) (Hong et al., 2003). Some studies have shown that the AMPK/sirtuin 1 (SIRT1)/peroxisome proliferator-activated receptor-γ coactivator 1α (PGC-1α) signaling pathway plays a crucial role in the protection of cardiac function by participating in energy metabolism, oxidative stress, and mitochondrial function (Chau et al., 2010; Tian et al., 2019). The aim of this study is to demonstrate that IVA may regulate mitochondrial energy metabolism and oxidative stress through the AMPK/SIRT1/PGC-1α signaling pathway in an I/R model of H9c2 cardiomyocytes.

Materials and Methods

Reagents and antibodies

IVA was purchased from Target Mol (Shanghai, China). The primary antibodies used for western blots were as follows: antibodies against total and phosphorylated AMPKα (1:1000) and SIRT1 (1:1000) were purchased from Cell Signaling Technology (Beverly, MA, USA). The antibody against PGC-1α (1:1000) was purchased from Abcam (Abcam Technology, Cambridge, UK). Tubulin-β was used as a loading control and detected using a monoclonal Tubulin-β antibody (1:500, Affinity Biosciences, USA). NAD$^+$, ATP disodium salt, ADP sodium salt, and 5'-AMP-Na$_2$ were all purchased from Sigma (Sigma Aldrich, St Louis, MO, USA).

Cell culture

H9c2 embryonic rat cardiomyocytes, acquired from the Chinese Academy of Sciences Shanghai Cell Bank, were cultured in complete high-glucose Dulbecco's Modified Eagle Medium (DMEM), containing 10% fetal bovine serum (FBS), in an atmosphere of 95% humidified air and 5% CO$_2$, at 37°C. Cells in the logarithmic growth phase were selected for all experiments. After reaching 80–90% confluence, cells were digested for 1–2 min with 0.25% trypsin and passaged at 1:3 every 2–3 days.

Establishment of a myocardial I/R damage model and cell grouping

H9c2 cells were selected for the establishment of an I/R model, as described previously by Kuznetsov et al. (2015). According to the method designated previously by Yang et al. (2015), experimental groups were switch from high-glucose DMEM to serum- and glucose-free anoxic media (139 mmol/L NaCl, 4.7 mmol/L KCl, 0.5 mmol/L MgCl$_2$, 10 mmol/L CaCl$_2$, and 5 mmol/L HEPES, pH 7.4) and were maintained in anaerobic conditions, at 37°C, for 8 h. Subsequently, the medium was replaced with DMEM containing 10% fetal bovine serum, and cells were cultured in an incubator containing 95% air and 5% CO$_2$, at 37°C, for 24 h, to mimic re-oxygenation (reperfusion) conditions. The control group consisted of cells that were constantly maintained in normal medium, without the hypoxic stimulus. Each IVA group was pretreated previously with IVA before being subjected to IRI model treatment.

Cell counting kit-8 (CCK-8) assay

Cell viability was determined using CCK-8 (Beyotime, Shanghai, China), according to the manufacturer's protocol. Briefly, the H9c2 cell suspension density was adjusted to 5×10^3 cells/well and seeded in 96-well plates for 24 h. Different concentrations (1, 10, 20, 100, and 200 μM) of IVA were added to the wells and incubated for the indicated times (2, 12, and 24 h). Cells were then subjected to the I/R injury (IRI) model. After inducing IRI in H9C2c cells, 10 μL of CCK-8 reagent was added to each well, and incubation was continued for 2 h, at 37°C, in a 5% CO$_2$ incubator. The absorbance value was measured at 450 nm using a Microplate Reader (Tecan M 1000, Swiss Confederation, Tecan company, German), and the experiment was repeated three times.

Apoptosis assay

To investigate the effects of IVA on H9c2 cell survival after I/R, we used flow cytometry combined with Annexin V and propidium iodide (PI) staining to evaluate the apoptosis rate of IRI model H9c2 cells treated with IVA. Flow cytometry analysis, using an Annexin V-FITC/PI Apoptosis Detection Kit (BD Biosciences, USA), was performed to quantify and identify the percentage of apoptotic H9c2 cells. The H9c2 cell suspension density was adjusted to 1×10^6 cells/well and seeded in 6 well-plates. After IRI treatment, cells were collected, washed twice with cold phosphate-buffered saline (PBS), and resuspended in 500 μL 1× binding buffer. Next, 5 μL Annexin-V and 5 μL PI were added to each group of cells for 15 min, under shading conditions, at room temperature. Subsequently, the treated cells were measured using a flow cytometer (Beckman Coulter, USA) to differentiate necrotic cells from apoptotic cells, according to the manufacturer's instructions, and the experiment was repeated three times.

Morphological examination of mitochondria by transmission electron microscopy

Cells were harvested and fixed with 2.5% glutaraldehyde (TED PELLA INC) for 12 h at 4°C. Change the 2.5% glutaraldehyde

to 0.01 M PBS-phosphate buffer (pH7.4) and process for 2 h. Cells were post-fixed with 0.1% osmium acid for 1 h (TED PELLA INC), dehydrated using an ethanol gradient series, and then soaked and embedded in pure epoxy resin (Fluka Analytical, Sigma). 70 nm-ultrathin sections were cut and placed on the copper grids. The sections on the grids were double-stained with uranyl acetate and lead citrate before being examined under transmission JEM1400 electron microscope (JEOL, Japan).

Mitochondrial stress assay
In this study, a biochemical analyzer was used to measure the oxygen consumption rate (OCR) and extracellular acidification rate (ECAR) of H9c2 cells after I/R treatment, and the related indicators were analyzed to determine the effects of IRI on cellular oxidative phosphorylation and glycolysis. A Seahorse XF24 Extracellular Flux Analyzer was used to determine a suitable inoculation density and the optimal carbonyl cyanide p-trifluoromethoxy phenylhydrazone (FCCP) concentration for use in normal H9c2 cells, according to the manufacturer's instructions. A mitochondrial stress assay was performed to evaluate the effects of IRI on mitochondrial OCR and ECAR. On the first day, H9c2 cells were plated on 24-well proprietary Seahorse Biosciences plates (2×10^5 cells/well), in 250 µL medium, and could adhere and grow overnight before the IRI experiments. Simultaneously, sensor cartridges (Seahorse) were hydrated in XF Calibrant, overnight, at 37°C, without CO_2. On the second day, the H9c2 growth medium was removed and replaced with assay medium, which was composed of unbuffered DMEM, supplemented with 25 mM D-glucose, 20 mM sodium pyruvate and 4 mM L-glutamine, pH 7.4. Then, H9c2 cells were incubated at 37°C, without CO_2, for 1 h prior to respiration analysis.

The OCR parameter values were measured after the injection of load compounds, including oligomycin (1 µM), FCCP (2 µM), antimycin (1 µM), and rotenone (1 µM) (Sigma) into the appropriate ports of a hydrated sensor cartridge from the XF Cell Mito Stress Test kit. The mitochondrial function parameters were automatically calculated by the Seahorse XF Mito Stress Test Report Generator. The ECAR measurement method was the same as that for OCR, except the reagents used were glucose (10 mM), oligomycin (1 µM), and 2-deoxyglucose (50 mM) (Seahorse Bioscience, 2009).

Measurement of ROS generation in H9c2 cells
ROS production has been demonstrated to play key roles during energy metabolism disorders and mitochondrial damage under IRI conditions. The effects of IVA on ROS production were investigated by exposing H9c2 cells to IRI conditions with or without IVA pretreatment. According to the ROS kit (Biosharp Co., Ltd., Guangzhou, China), intracellular ROS can oxidize non-fluorescent 2',7'-dichlorodihydrofluorescein diacetate (DCF-DA) to generate fluorescent 2',7'-dichlorofluorescein (DCF), which can be measured to determine ROS production. H9c2 cells were washed twice with PBS after receiving the designated treatment and were then incubated with a suitable amount of DCF-DA solution, at a final concentration of 10 µM, in a

37°C incubator, for 30 min. DCF fluorescence was measured in the field of view, using laser scanning confocal microscopy (Carl Zeiss, German), after washing three times with serum-free medium. Four random fields of view were selected by two investigators, and their mean fluorescence intensities were analyzed using Image-J software to indicate the level of ROS.

ATP, ADP, AMP, and NAD$^+$ content measurement with HPLC
High-performance liquid chromatography (HPLC) was applied to determine the ATP, ADP, AMP, and NAD$^+$ contents (Garcia-Tardon and Guigas, 2018). Chromatographic conditions were as follows. HypersilTM ODS-2 (C18) HPLC (5.0 µm, 4.6 × 250 mm). Mobile phase: 0.5% methanol, 99.5% phosphate buffer (10 mmol/L KH_2PO_4, pH 7.0). Flow rate: 1.0 mL/min. Column temperature: 30°C. Detection wavelength: 259 nm. Injection volume: 20 µL. The retention time was used to determine the quality, and the peak area was used to determine the quantity. H9c2 cells were collected in 0.2 mL PBS and lysed by repeated freezing and thawing (3 times, 30 min each). Then, 0.2 mL $HClO_4$ solution (0.5 M) was added, and the pH of the supernatant was adjusted to 7.0. The cells were centrifuged for 25 min, at 4°C, at 12000 rpm. Then, 20 µL of each sample was injected into the HPLC system to identify and analyze the ATP, ADP, AMP, and NAD$^+$ contents.

Western blot
Treated cells were washed with pre-cooled PBS, lysed with 100 µL RIPA buffer (Beyotime, China), supplemented with phosphatase inhibitor and protease inhibitor, and incubated on ice for 30 min. Then, the lysed cells were collected and centrifuged at 13200 rpm for 25 min. The supernatant was collected, the protein concentration was measured using a BCA protein assay kit (Beyotime, China), and the sample was denatured by boiling for 10 min. Proteins were separated using sodium dodecyl sulfate-polyacrylamide gel electrophoresis (SDS-PAGE) and transferred to a polyvinylidene difluoride (PVDF) membrane. After blocking with 5% milk, the membrane was incubated with antibodies against AMPK (1:1000, Cell Signaling Technology, Inc.), p-AMPK (1:1000, Cell Signaling Technology, Inc.), SIRT1 (1:1000, Cell Signaling Technology, Inc.), PGC-1α (1:500, Abcam), Glut4 (1:500, Affinity), and Tubulin-β (1:1000, Affinity), at 4°C, overnight. After washing three times with Tris-buffered saline containing Tween 20 (TBST), membranes were incubated with the corresponding secondary antibodies for 1 h at room temperature. After washing three times with TBST, the bound antibody was observed using an enhanced chemiluminescent substrate (Image Lab).

Real-time reverse transcription-polymerase chain reaction (RT-PCR)
Total RNA was extracted from the H9c2 cells, using an RNA kit (QIAGEN, Germany), according to the manufacturer's instructions. The reverse transcription reaction was performed using a cDNA synthesis kit (Thermo, USA). The mRNA levels, relative to *actin* mRNA levels, were determined using a real-time quantitative PCR analyzer (QIAGEN,

Germany). The primer sequences (Shanghai Sangon Biological Engineering Co., Ltd., Shanghai, China) were as follows:

AMPK sense: 5'-AAG ATC GGA CAC TAC GTG CT-3'; AMPK antisense: 5'-CTG CCA CTT TAT GGC CTG TC-3'; SIRT1 sense: 5'-TTT ATG CTC GCC TTG CTG TG-3'; SIRT1 antisense: 5'-AGA GAT GGC TGG AAC TGT CC-3'; PGC-1α sense: 5'-TGG GTG GAT TGA AGT GGT GT-3'; PGC-1α antisense: 5'-CGC TGA CAA GTT TGC CTC AT-3'; Actin sense: 5'-TGG AAT CCT GTG GCA TCC ATG AAA C-3'; Actin antisense: 5'-ACG CAG CTC AGT AAC AGT CCG-3'.

Statistical analysis
All data are presented as the mean ± standard deviation (SD) and were analyzed using SPSS 20.0 software and Prism 8.0 software. Differences among groups were analyzed with Student's *t*-test and one-way analysis of variance (ANOVA). $p < 0.05$ was considered to be significant.

Results

Effects of IRI on energy metabolism in H9c2 cells under physiological conditions
As shown in Figs. 1A and 1C, the optimal H9c2 cell volume was 2.0×10^4, and the optimal concentration of FCCP was 2 μM. When mitochondrial bioenergy metabolism indicators were analyzed, the results showed that the basal respiration (*$p < 0.05$) and ATP production (**$p < 0.01$) were reduced, and proton leakage was increased (**$p < 0.01$) in IRI cells compared with uninjured cells (Fig. 1B). These

results indicate that IRI largely inhibits the process of mitochondrial energy metabolism. Simultaneously, to adapt to the hypoxic environment, the glycolytic capacity (*$p < 0.05$), glycolytic reserves (*$p < 0.05$), and glycolytic reserves (%) (**$p < 0.01$), were significantly increased and glycolysis was reduced (**$p < 0.01$) in IRI cells (Fig. 1D).

IVA treatment increases H9c2 cell survival rate after IRI
During the CCK8 assay, H9c2 cells were incubated with different concentrations (0, 1, 10, 20, 100, and 200 μM) of IVA for 2, 12, and 24 h. As shown in Fig. 2A, a significant protective effect was observed for cell proliferation when IVA pretreatment lasted at least 12 h, and the concentration was maintained between 20 and 100 μM ($c = 20$ μM, *$p < 0.05$; and $c = 100$ μM, **$p < 0.01$). Therefore, pretreatments with either 20 or 100 μM IVA, for 12 h, were used during subsequent experiments. Flow cytometry analysis revealed that the proportion of late apoptotic cells in the IRI group was significantly reduced by IVA pretreatment, suggesting that IVA may play a role in the prevention of apoptosis in the IRI model (Fig. 2B).

Effects of IVA on mitochondrial morphology in myocardial cells after IRI
Electron microscopy results showed that the myocardial cell structure was severely damaged in the IRI group, and many vacuole-like structures were observed. The mitochondria became rounded, swollen, smashed, or even disappeared, and the matrix density deepened (Figs. 3A and 3B). IVA treatment improved the mitochondrial structure damage
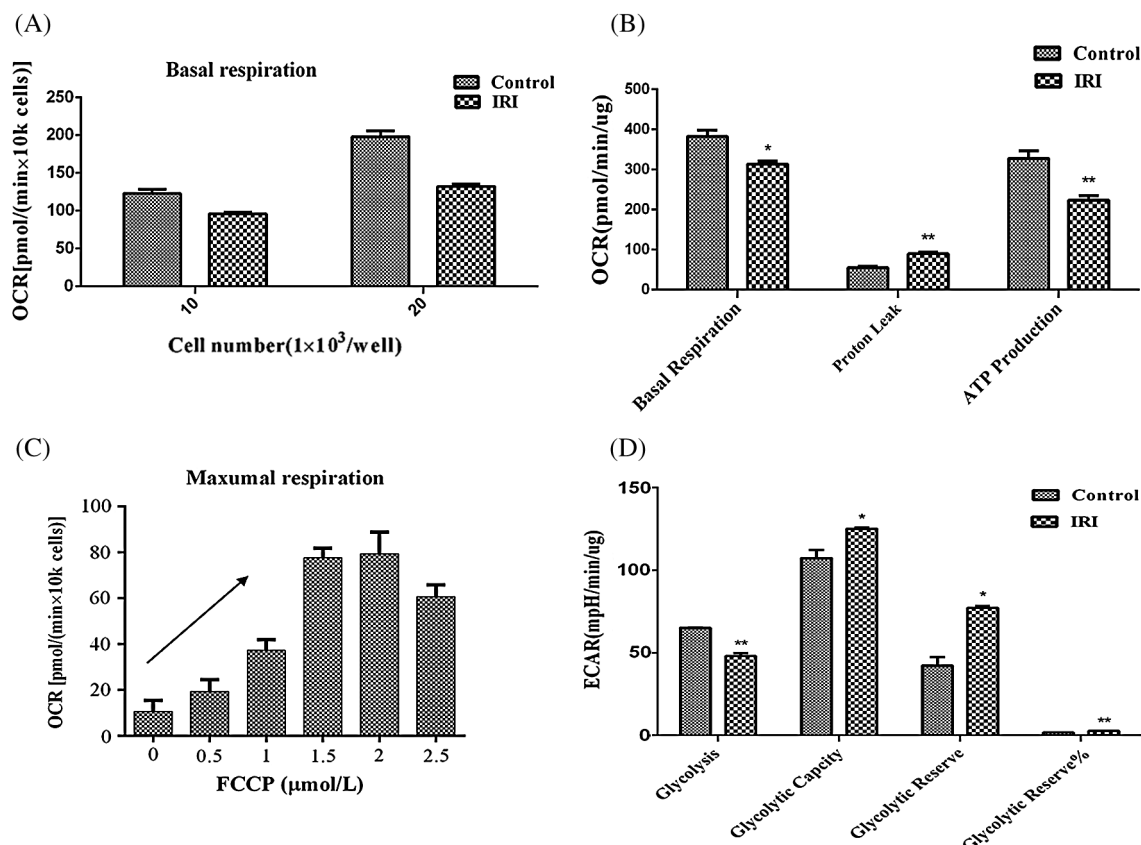

FIGURE 1. Bioenergy metabolism of H9c2 cells after IRI. (A) Basal respiration rates at various cell densities. (B) Alterations in basal respiration, proton leak, and ATP production in response to IRI treatment. (C) Maximal respiration rates of cells treated with gradient concentrations of FCCP (0, 0.5, 1.0, 1.5, 2.0, and 2.5 μM). (D) Alterations in glycolysis, glycolytic capacity, glycolytic reserve, and glycolytic reserve% in response to IRI treatment. Compared with the control group, *$p < 0.05$, **$p < 0.01$.
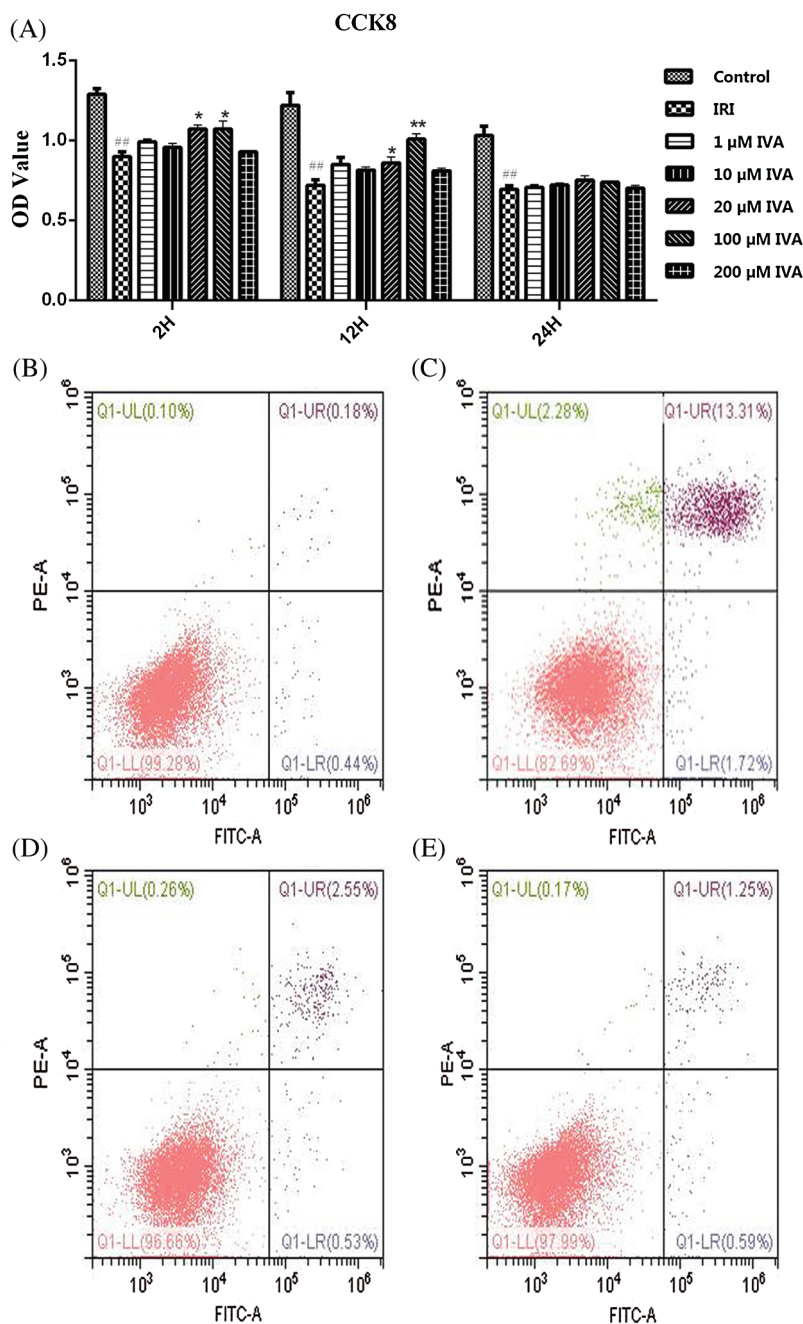
FIGURE 2. Effect of IVA pretreatment on the H9c2 cell survival rate after IRI induction. (A) Effects on cell proliferation when H9c2 cells were pretreated with different IVA concentrations (1, 10, 20, 100, and 200 μM) for 2, 12, and 24 h prior to IRI, as assessed by the CCK-8 assay. (B) Apoptosis rate of control group. (C) Apoptosis rate of IRI group. (D) Apoptosis rate of IVA 20 μM group. (E) Apoptosis rate of IVA 100 μM group. Data are expressed as the mean ± SD, N ≥ 3. Compared with the control group, $^{\#}p < 0.05$, $^{\#\#}p < 0.01$. Compared with the IRI group, $^{*}p < 0.05$, $^{**}p < 0.01$. (B) IVA had a significant protective effect against apoptosis in H9c2 cells after I/R, as assessed by flow cytometry.

induced by IRI to a certain degree. In particular, mitochondria treated with IVA at a concentration of 100 μM tended to reduce swollen and vacuole. Moreover, the matrix color was reduced, and the bilayer membrane was relatively intact (Figs. 3C and 3D).

IVA inhibits the IRI-induced effects on ATP, ADP, AMP, NAD⁺ contents and on the AMP/ATP ratio in H9c2 cardiomyocytes

As shown in Figs. 4A and 4B, the retention times for ATP, ADP, AMP, and NAD$^+$ were 2.6, 3.2, 4.5, and 14.3 min, respectively. The standard curve equation was obtained using the linear regression from the peak area (Y), for ATP, ADP, AMP, and NAD$^+$, to the concentration (X) (Fig. 4C).

The evaluation of the intracellular ATP, ADP, and AMP levels showed that IVA treatment protected the mitochondrial function of H9c2 cells by increasing ATP production and decreasing the ADP and AMP contents. The AMP/ATP ratio decreased significantly in IVA treated cells compared with untreated cells (Figs. 4D and 4E). The exposure of H9c2 cells to IRI significantly reduced ATP generation ($^{\#\#}p < 0.01$), which was reversed by pre-treatment with IVA (20 or 100 μM) for 12 h ($^{**}p < 0.01$). Additionally, IVA treatments at either 20 or 100 μM abrogated the IRI-induced decrease in NAD$^+$ generation ($c = 20$ μM, $^{*}p < 0.05$; and $c = 100$ μM, $^{**}p < 0.01$). These data suggested that IVA maintained mitochondrial function by upregulating ATP and NAD$^+$ expression.

IVA mitigates IRI-induced ROS production

The antioxidant potential of IVA against intracellular ROS generation was investigated using the DCF-DA assay. The production of ROS following the IRI of H9c2 cells was measured in the absence or presence of IVA (20 and 100 μM).
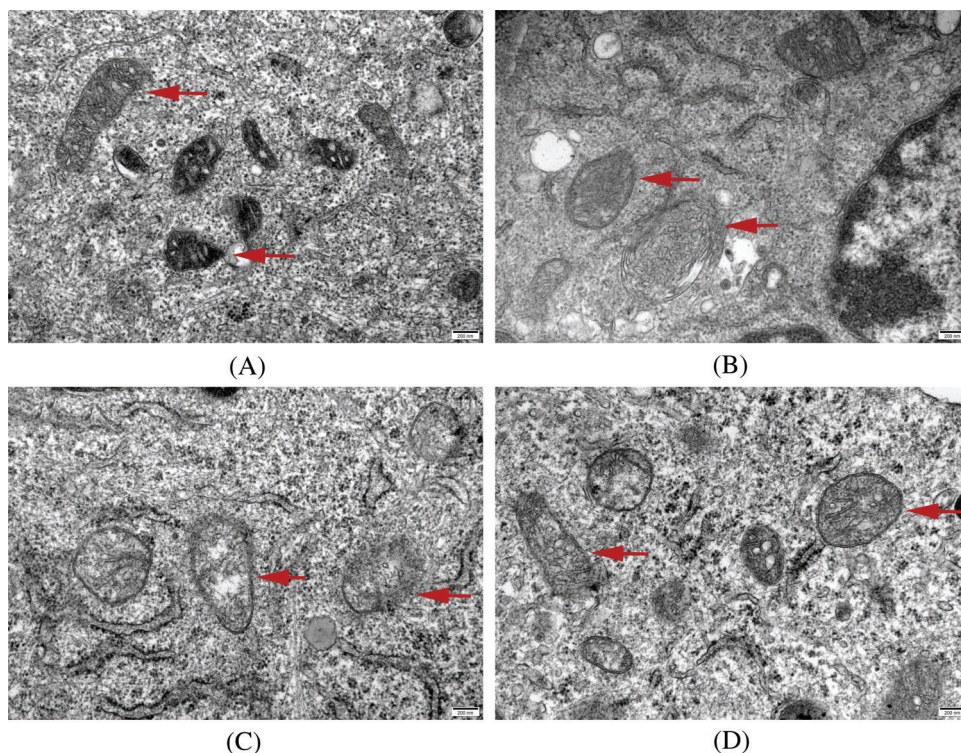
FIGURE 3. Effect of IVA on mitochondrial morphology in H9c2 cells after IRI (200×). (A) The mitochondrial morphology of the control group. (B) The mitochondrial morphology of the IRI group. (C) The mitochondrial morphology of the 20 μM IVA group. (D) The mitochondrial morphology of the 100 μM IVA group. Red arrows indicate the morphological changes in mitochondria after and before IRI induction.

As shown in Figs. 5A and 5B, the amount of intracellular ROS generation in the IRI model group increased significantly relative to that in the control group, indicating that the model successfully induced oxidative stress ($^{##}p < 0.01$). As shown in Figs. 5C and 5D, IVA treatment reduced IRI-induced ROS production ($c = 20$ μM, $^*p < 0.05$; and $c = 100$ μM, $^{**}p < 0.01$).

IVA pretreatment effect on AMPK, SIRT1, and PGC-1α mRNA expression after IRI induced in H9C2c cells
The RT-PCR analysis (Fig. 6) indicated that IRI reduced the expression levels of SIRT1 and PGC-1α mRNA at the mRNA level, which was reversed by IVA ($c = 20$ μM, $^*p < 0.05$; and $c = 100$ μM, $^{**}p < 0.01$). These results were consistent with previous findings, which confirm the downregulation of NAD^+ improved by IVA pretreatment in IRI induced in H9c2 cardiomyocytes. Additionally, no significant change in the expression levels of AMPK mRNA was observed ($p > 0.05$).

IVA activates the AMPK/SIRT1/PGC-1α signaling pathway
As shown in Fig. 7, in comparison with the IRI group, the IVA-treated group showed increased AMPK activation ($c = 20$ μM, $^*p < 0.05$; and $c = 100$ μM, $^*p < 0.01$). The expression levels of SIRT1 and PGC-1α decreased in H9c2 cardiomyocytes induced by IRI. However, a significant recovery of their expression levels was observed by IVA pretreatment.

Discussion

Our study indicated that the bioenergy metabolism characteristics of myocardial cells are altered after IRI. In addition to relieving mitochondrial damage, the administration of IVA improved cell energy metabolism,

reduced oxidative stress, increased cell viability, and inhibited cardiomyocyte apoptosis. The experimental results showed that this protection was closely related to the AMPK/SIRT1/PGC-1α signaling pathway. IVA reduces oxidative stress and improves myocardial mitochondrial energy metabolism by regulating the AMPK/SIRT1/PGC-1α signaling pathway in the H9c2 cardiomyocyte IRI model.

During myocardial IRI, energy metabolism disorder causes hypoxia-reperfusion injury (Gary and Edmonton, 2000). Reperfusion is characterized by an early and a late phase, during which, due to reduced adenylate cyclase activity and intracellular cAMP levels, free radicals, such as ROS, are generated. The mechanisms of cell death are triggered; ROS can further aggravate existing tissue damage (Lei *et al.*, 2015). The beta-blocker esmolol reduces myocardial damage after resuscitation by regulating apoptosis, acting as an antioxidant, and improving energy metabolism (Zhang and Li, 2013). Preclinical studies have suggested that reductions in ROS formation, caused by the inhibition of NADPH oxidase, may be the underlying mechanism through which IVA confers cardioprotection. IVA reduced myocardial cell injury by decreasing ROS bursts during the period of reperfusion (Bolli *et al.*, 2013; Heusch, 2009). This evidence suggests that IVA may also have a cardioprotective mechanism that mitigates IRI by protecting cardiomyocyte mitochondrial function, especially mitochondria-mediated cellular energy metabolism and oxidative stress.

Mitochondria are considered to act as the energy pool for cardiomyocytes and are directly related to energy metabolism. Mitochondrial changes are closely related to myocardial damage, such as changes in mitochondrial structure, biosynthesis abnormalities, the excessive accumulation of ROS, and the excessive consumption of NAD^+ (Ong *et al.*,
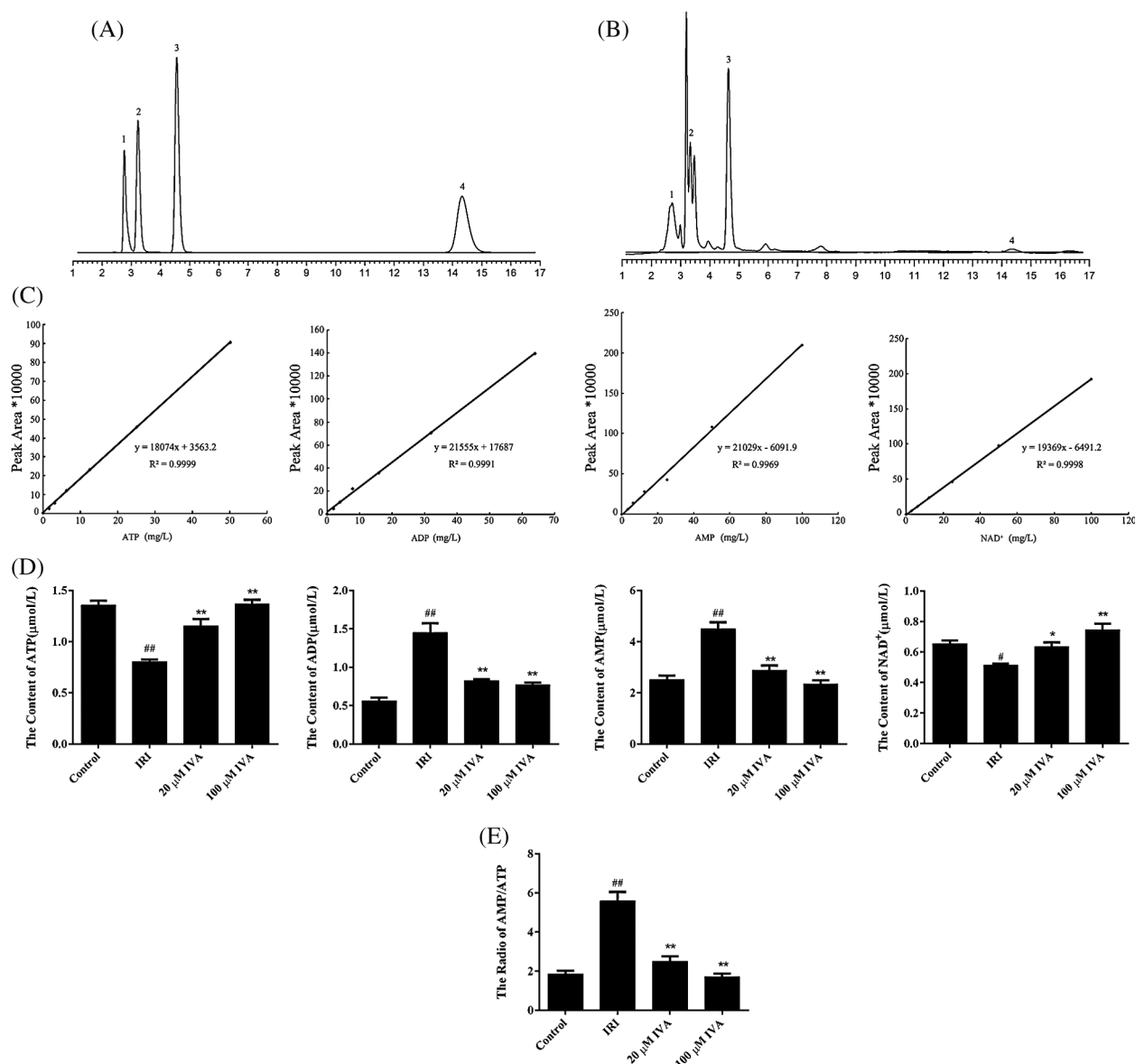
FIGURE 4. Effects of IVA on the ATP, ADP, AMP, and NAD$^+$ contents in H9c2 cells after IRI. (A) HPLC chromatogram of the standard sample 1 = ATP, 2 = ADP, 3 = AMP, and 4 = NAD$^+$. (B) HPLC chromatogram of the H9c2 cell sample, 1 = ATP, 2 = ADP, 3 = AMP, and 4 = NAD$^+$. (C) The standard curve for ATP, ADP, AMP, and NAD$^+$. (D) The effects of IVA on the ATP, ADP, AMP, and NAD$^+$ contents in H9c2 cells after IRI. (E) The effects of IVA on the AMP/ATP ratio. All data are expressed as the mean ± SD, N ≥ 3. Compared with the control group, $^{\#}p < 0.05$, $^{\#\#}p < 0.01$. Compared with the IRI group, $^{*}p < 0.05$, $^{**}p < 0.01$.

2013; Pei *et al.*, 2016; Di Lisa *et al.*, 2001; Fujio *et al.*, 2011). The activation of the AMPK signaling pathway is a MIRI protection mechanism, with important pathophysiological significance, and represents one of the signaling pathways that has been increasingly explored in a recent study focused on MIRI (Qi and Young, 2015).

During I/R, the available oxygen and ATP production in the myocardium is insufficient, leading to the accumulation of ADP and AMP and an increase in the AMP/ATP ratio. AMPK becomes activated when AMP binds with the regulatory nucleotide-binding domain of the AMPK gamma subunit (Salt and Hardie, 2017). Activated AMPK regulates many downstream molecules and reduces MIRI by optimizing myocardial energy metabolism, inhibiting oxidative stress, apoptosis, and regulating autophagy and anti-inflammatory activities (Daskalopoulos *et al.*, 2016; Qi and Young, 2015). During ischemia, SIRT1 mediates AMPK activation, and in

turn, AMPK regulates SIRT1 activity by regulating NAD$^+$ levels (Ruderman *et al.*, 2010; Wang *et al.*, 2018). In addition, AMPK and SIRT1 cooperate to activate the expression of PGC-1α which can effectively resist cellular oxidative stress. The upregulation of PGC-1α can reduce oxidative stress damage, however the downregulation of PGC-1α directly affects mitochondrial dysfunction (Ham and Raju, 2017). This study showed the increased activation of AMPK (p-AMPK) in cells after IRI, and IVA further increased p-AMPK levels, suggesting that IVA can upregulate p-AMPK expression. Meanwhile, the expression levels of SIRT1 and PGC-1α mRNA and protein with the intracellular ATP levels, were also significantly upregulated by IVA treatment. Some studies have confirmed that the AMPK/SIRT1/PGC-1α signaling pathway plays a crucial role during energy metabolism and oxidative stress which are closely related to the protection of cardiac function
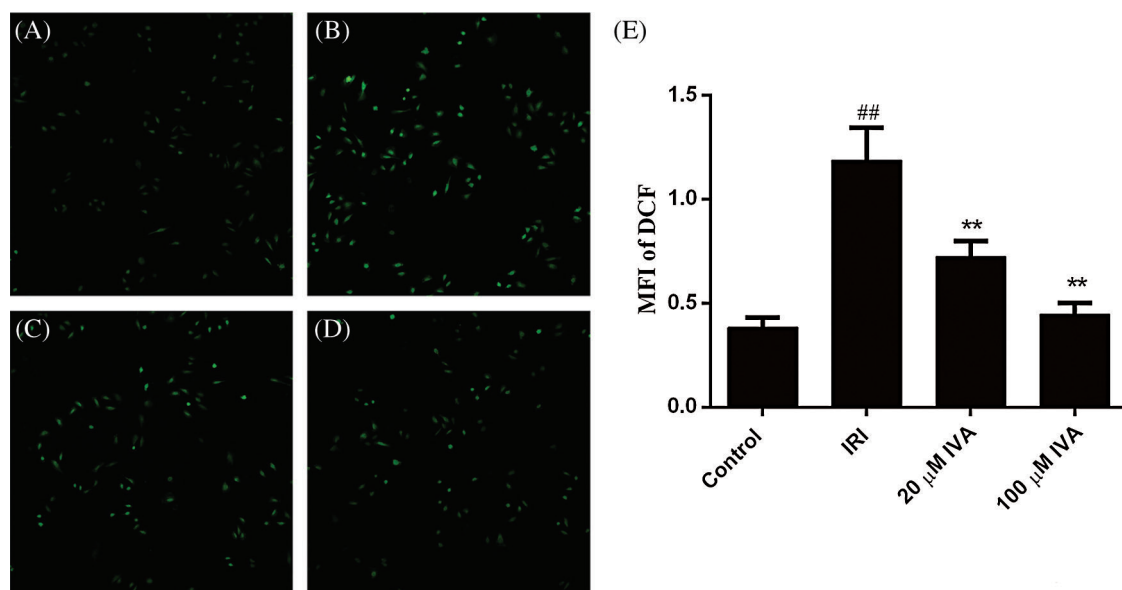
FIGURE 5. Assessment of intracellular ROS production by DCF-DA staining in injured H9c2 cells and pretreated with IVA. (A) Control group. (B) H9c2 cells subjected to IRI treatment. (C) H9c2 cells pre-treated with 20 µM IVA for 12 h prior to IRI treatment. (D) H9c2 cells pre-treated with 100 µM IVA for 12 h prior to IRI treatment. (E) Quantitative analysis of the mean fluorescence intensity (MFI) of DCF using ImageJ 1.41 software. All data are expressed as the mean ± SD, N ≥ 3. Compared with the control group, [#]$p < 0.05$, [##]$p < 0.01$. Compared with the IRI group, [*]$p < 0.05$, [**]$p < 0.01$.
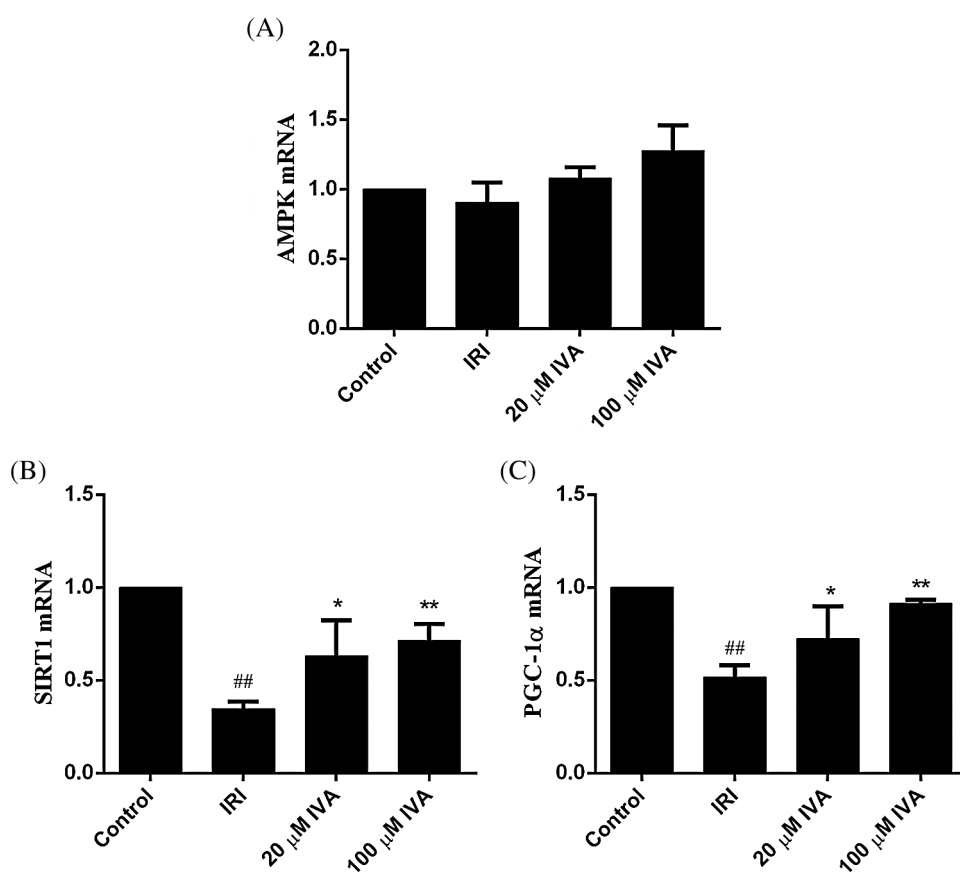

FIGURE 6. Effect of IVA pretreatment on the expression levels of AMPK, SIRT1, and PGC-1α mRNA after IRI induced in H9c2 cells. All data are expressed as the mean ± SD, N ≥ 3. Compared with the control group, [#]$p < 0.05$, [##]$p < 0.01$. Compared with the IRI group, [*]$p < 0.05$, [**]$p < 0.01$.

(Chau et al., 2010; Tian et al., 2019). Therefore, the protective effects of IVA may be related to the AMPK/SIRT1/PGC-1α signaling pathway.

Currently, many pharmacological functions for IVA have been reported (Xiang et al., 2019; Yu et al., 2018). For example, IVA was shown to prevent cartilage matrix degradation caused by inflammation and oxidative stress. IVA also alleviated cardiac fibrosis and hypertrophy via the PI3K/AKT/mTOR/p70S6K pathway. In clinical studies, intravenous IVA after percutaneous coronary interventions (PCIs), performed after ST-elevation myocardial infarction (STEMI), was associated with notable reductions in left
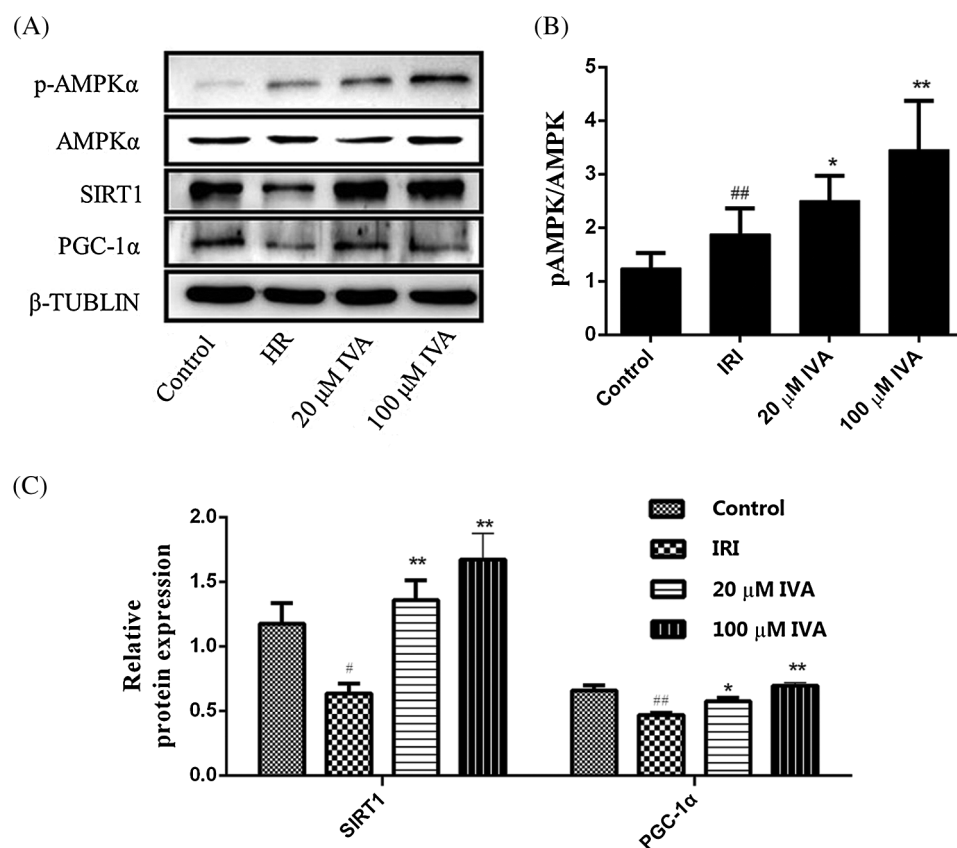
FIGURE 7. Effect of IVA pretreatment on the expression levels of AMPK, SIRT1 and PGC-1α proteins after IRI induced in H9c2 cells. (A) The expression levels of p-AMPK, AMPK, SIRT1, and PGC-1α proteins in H9c2 cells after IRI. (B) Graph showing the p-AMPK/AMPK ratios. (C) Graph showing the relative protein expression levels of SIRT1 and PGC-1α. All data are expressed as the mean ± SD, N ≥ 3. Compared with the control group, [#]$p < 0.05$, [##]$p < 0.01$. Compared with the IRI group, [*]$p < 0.05$, [**]$p < 0.01$.

ventricular ESV and EDV when compared with placebo treatments (Steg et al., 2013). In addition, IVA was associated with an improved left ventricular remodeling in reperfused STEMI patients, based on cardiac magnetic resonance assessments (Gerbaud et al., 2014). These findings showed that the mechanism of action underlying IVA cardioprotection may be more complex because IVA may have a wide range of clinical applications. Myocardial disorders after cardiac arrest and resuscitation are associated with high mortality after resuscitation (Herlitz et al., 1995; Laver et al., 2004). Our study examined the beneficial mechanisms underlying IVA treatment, thus identifying novel mechanisms and potential targets associated with the protection of the mitochondrial bioenergetic process for the development of future PRMD treatments.

Limitations

This study had the following limitations. First, this study only illustrated the effect of IVA on aerobic phosphorylation. Whether IVA can improve myocardial I/R effects associated with the anaerobic oxidation of glucose and increased anaerobic glycolysis remains unknown. Further investigation of these aspects is worthy of an in-depth study in the future. Second, this study did not use signaling pathway inhibitors to confirm the link between IVA and the AMPK/SIRT1/PGC-1α signaling pathway. Third, this study only examined the role of the AMPK/SIRT1/PGC-1α signaling pathway, which may not be the only pathway through which IVA affects PRMD. Therefore, further research is necessary in the future to elucidate these questions.

Conclusions

In conclusion, IVA can protect against myocardial energy metabolism disorders and reduce oxidative stress, ultimately improving myocardial function. The effects of IVA may be regulated by the AMPK/SIRT1/PGC-1α signaling pathway. Compared with traditional heart-rate-lowering beta-blockers, IVA represents a viable and innovative treatment option for reducing mortality after CPR, and it may have a wider range of clinical applications beyond the treatment of cardiac disorders.

Author Contributions: M.Y. conceptualized the experiments, interpreted the results, and prepared the manuscript. X.Z., T.H., and M.W. performed the experiments and helped to prepare the manuscript. J.W. and J.H. helped to perform the experiments.

Availability of Data and Materials: The datasets used or analysed during the current study are available from the corresponding author on reasonable request.

References

Seahorse Bioscience. (2009). *XF24 ExtracellularFlux Analyzer And Prep Station*. Billerica, MA: Seahorse Bioscience.

Bolli R, Patel BS, Jeroudi MO, Lai EK, McCay PB (2013). Demonstration of free radical generation in stunned myocardium of intact dogs with the use of the spin trap α-phenyl N-tert-butyl nitrone. *Journal of Clinical Investigation* 82: 476–485. DOI 10.1172/JCI113621.

Chau MDL, Gao J, Yang Q, Wu Z, Gromada J (2010). Fibroblast growth factor 21 regulates energy metabolism by activating the AMPK-SIRT1-PGC-1α pathway. *Proceedings of the National Academy of Sciences of the United States of America* 107: 12553–12558. DOI 10.1073/pnas.1006962107.

Custodis F, Baumhäkel M, Schlimmer N, List F, Gensch C, Böhm M, Laufs U (2008). Heart rate reduction by ivabradine reduces oxidative stress, improves endothelial function, and prevents atherosclerosis in apolipoprotein E-deficient mice. *Circulation* 117: 2377–2387. DOI 10.1161/CIRCULATIONAHA.107.746537.

Daskalopoulos EP, Dufeys C, Bertrand L, Beauloye C, Horman S (2016). AMPK in cardiac fibrosis and repair: actions beyond metabolic regulation. *Journal of Molecular and Cellular Cardiology* 91: 188–200. DOI 10.1016/j.yjmcc.2016.01.001.

Yellon DM, Hausenloy DJ (2007). Myocardial reperfusion injury. *New England Journal of Medicine* 357: 1121–1135. DOI 10.1056/NEJMra071667.

Di Lisa F, Menabo R, Canton M, Barile M, Bernardi P (2001). Opening of the mitochondrial permeability transition pore causes depletion of mitochondrial and cytosolic NAD$^+$ and is a causative event in the death of myocytes in postischemic reperfusion of the heart. *Journal of Biological Chemistry* 276: 2571–2575. DOI 10.1074/jbc.M006825200.

Fasullo S, Cannizzaro S, Maringhini G, Ganci F, Giambanco F, Vitale G, Pinto V, Migliore G, Torres D, Sarullo FM, Paterna S, Di Pasquale P (2009). Comparison of ivabradine versus metoprolol in early phases of reperfused anterior myocardial infarction with impaired left ventricular function: preliminary findings. *Journal of Cardiac Failure* 15: 856–863. DOI 10.1016/j.cardfail.2009.05.013.

Fujio Y, Maeda M, Mohri T, Obana M, Iwakura T, Hayama A, Yamashita T, Nakayama H, Azuma J (2011). Glycoprotein 130 cytokine signal as a therapeutic target against cardiovascular diseases. *Journal of Pharmacological Sciences* 117: 213–222. DOI 10.1254/jphs.11R05CR.

Garcia-Tardon N, Guigas B (2018). Determination of adenine nucleotide concentrations in cells and tissues by high-performance liquid chromatography. *Methods Molecular Biology* 1732: 229–237.

Gary L, Edmonton A (2000). Regulation of carbohydrate metabolism in ischemia and reperfusion. *American Heart Journal* 139: 115–119. DOI 10.1067/mhj.2000.103919.

Gerbaud E, Montaudon M, Chasseriaud W, Gilbert S, Cochet H, Pucheu H, Horovitz A, Bonnet J, Douard H, Coste P (2014). Effect of ivabradine on left ventricular remodelling after reperfused myocardial infarction: a pilot study. *Archives of Cardiovascular Diseases* 107: 33–41. DOI 10.1016/j.acvd.2013.12.001.

Ham PB, Raju R (2017). Mitochondrial function in hypoxic ischemic injury and influence of aging. *Progress in Neurobiology* 157: 92–116. DOI 10.1016/j.pneurobio.2016.06.006.

Herlitz J, Ekstrtim L, Wennerblom A, Axelsson AB, Holmberg S (1995). Hospital mortality after out-of-hospital cardiac arrest among patients found in ventricular fibrillation. *Resuscitation* 29: 11–21. DOI 10.1016/0300-9572(94)00811-S.

Heusch G (2009). A beautiful lesson—ivabradine protects from ischaemia, but not from heartfailure: through heart rate reduction or more? *European Heart Journal* 30: 2300–2301. DOI 10.1093/eurheartj/ehp360.

Hong SP, Leiper FC, Woods A, Carling D, Carlson M (2003). Activation of yeast Snf1 and mammalian AMP-activated protein kinase by upstream kinases. *Proceeding of the National Academy of Sciences of the United States of America.* 100: 8839–8843.

Jentzer JC, Chonde MD, Dezfulian C (2015). Myocardial dysfunction and shock after cardiac arrest. *BioMed Research International* 2015: 1–14. DOI 10.1155/2015/314796.

Ji XF, Shuo W, Yang L, Li CS (2012). Impaired β-adrenergic receptor signalling in post-resuscitation myocardial dysfunction. *Resuscitation* 83: 640–644. DOI 10.1016/j.resuscitation.2011.11.014.

Kleinbongard P, Gedik N, Witting P, Freedman B, Klöcker N, Heusch G (2015). Pleiotropic, heart rate-independent cardioprotection by ivabradine. *British Journal of Pharmacology* 172: 4380–4390. DOI 10.1111/bph.13220.

Kuwabara Y, Kuwahara K, Takano M, Kinoshita H, Arai Y, Yasuno S, Nakagawa Y, Igata S, Usami S, Minami T, Yamada Y, Nakao K, Yamada C, Shibata J, Nishikimi T, Ueshima T, Nakao T (2013). Increased expression of hcn channels in the ventricular myocardium contributes to enhanced arrhythmicity in mouse failing hearts. *Journal of the American Heart Association* 2: e000150. DOI 10.1161/JAHA.113.000150.

Kuznetsov AV, Javadov S, Sickinger S, Frotschnig S, Grimm M (2015). H9c2 and HL-1 cells demonstrate distinct features of energy metabolism, mitochondrial function and sensitivity to hypoxia-reoxygenation. *Biochimica et Biophysica Acta (BBA)-Molecular Cell Research* 1853: 276–284. DOI 10.1016/j.bbamcr.2014.11.015.

Laver S, Farrow C, Turner D, Nolan J (2004). Mode of death after admission to an intensive care unit following cardiac arrest. *Intensive Care Medicine* 30: 2126–2128. DOI 10.1007/s00134-004-2425-z.

Lei XM, Chao HL, Zhang Z, Lv JR, Li S, Wei HD, Xue RL, Li F, Li ZF (2015). Neuroprotective effects of quercetin in a mouse model of brain ischemic/reperfusion injury via anti-apoptotic mechanisms based on the Akt pathway. *Molecular Medicine Reports* 12: 3688–3696. DOI 10.3892/mmr.2015.3857.

Li YC, Luo Q, Ge LS, Chen YH, Zhou ND, Zhang T, Guan XQ, Lin JF (2013). Ivabradine inhibits the production of proinflammatory cytokines and inducible nitric oxide synthase in acute coxsackievirus B3-induced myocarditis. *Biochemical and Biophysical Research Communications* 431: 450–455. DOI 10.1016/j.bbrc.2012.12.147.

Link MS, Berkow LC, Kudenchuk PJ, Halperin HR, Hess EP, Moitra VK, Neumar RW, O'Neil BJ, Paxton JH, Silvers SH,

White RD, Yannopoulos D, Donnino MW (2015). Part 7: adult advanced cardiovascular life support: 2015 American Heart Association guidelines update for cardiopulmonary resuscitation and emergency cardiovascular care. *Circulation* **132**: S444–S464. DOI 10.1161/CIR.0000000000000261.

Marazia S, Urso L, Contini M, Pano M, Zaccaria S, Lenti V, Sarullo FM, Di Mauro M (2015). The role of Ivabradine in cardiac rehabilitation in patients with recent coronary artery bypass graft. *Journal of Cardiovascular Pharmacology and Therapeutics* **20**: 547–553. DOI 10.1177/1074248415575963.

Oliphant CS, Owens RE, Bolorunduro OB, Jha SK (2016). Ivabradine: a review of labeled and off-label uses. *American Journal of Cardiovascular Drugs* **16**: 337–347. DOI 10.1007/s40256-016-0178-z.

Ong SB, Hall AR, Hausenloy DJ (2013). Mitochondrial dynamics in cardiovascular health and disease. *Antioxidants & Redox Signaling* **19**: 400–414. DOI 10.1089/ars.2012.4777.

Ovize M, Baxter GF, Di Lisa F, Ferdinandy P, Garcia-Dorado D, Hausenloy DJ, Heusch G, Vinten-Johansen J, Yellon DM, Schulz R (2010). Postconditioning and protection from reperfusion injury: Where do we stand? Position paper from the working group of cellular biology of the heart of the European society of cardiology. *Cardiovascular Research* **87**: 406–423. DOI 10.1093/cvr/cvq129.

Palmer BS, Hadziahmetovic M, Veci T, Angelos MG (2004). Global ischemic duration and reperfusion function in the isolated perfused rat heart. *Resuscitation* **62**: 97–106. DOI 10.1016/j.resuscitation.2003.12.027.

Pei H, Yang Y, Zhao H, Li X, Yang D, Li D, Yang Y (2016). The role of mitochondrial functional proteins in ROS production in ischemic heart diseases. *Oxidative Medicine and Cellular Longevity* **2016**: 1–8. DOI 10.1155/2016/5470457.

Qi D, Young LH (2015). AMPK: energy sensor and survival mechanism in the ischemic heart. *Trends in Endocrinology & Metabolism* **26**: 422–429. DOI 10.1016/j.tem.2015.05.010.

Ruderman NB, Xu XJ, Nelson L, Cacicedo JM, Saha AK, Lan F, Ido Y (2010). AMPK and SIRT1: a long-standing partnership? *American Journal of Physiology Endocrinology and Metabolism* **298**: E751–E760. DOI 10.1152/ajpendo.00745.2009.

Salt IP, Hardie DG (2017). AMP-activated protein kinase: an ubiquitous signaling pathway with key roles in the cardiovascular system. *Circulation Research* **120**: 1825–1841. DOI 10.1161/CIRCRESAHA.117.309633.

Steg PG, Lopez-de-Sà E, Schiele F, Hamon M, Meinertz T, Goicolea J, Werdan K, Lopez-Sendon JL, on behalf of the VIVIFY (eValuation of the IntraVenous If inhibitor ivabradine after STsegment elevation mYocardial infarction) investigators. (2013). Safety of intravenous ivabradine in acute ST-segment elevation myocardial infarction patients treated with primary percutaneous coronary intervention: a randomized, placebo-controlled, double-blind, pilot study. *European Heart Journal-Acute Cardiovascular Care* **2**: 270–279. DOI 10.1177/2048872613489305.

Tian L, Cao W, Yue R, Yuan Y, Guo X, Qin D, Xing J, Wang X (2019). Pretreatment with Tilianin improves mitochondrial energy metabolism and oxidative stress in rats with myocardial ischemia/reperfusion injury via AMPK/SIRT1/PGC-1 alpha signaling pathway. *Journal of Pharmacological Sciences* **139**: 352–360. DOI 10.1016/j.jphs.2019.02.008.

Treptau J, Jeske O, Napp C, Menon O, Schieffer B, Schaefer A, Bauersachs J, Tongers J (2015). Ivabradine in acute heart failure: a therapeutic means for effective heart rate control. *Circulation* **132**: A18267.

Trivi M, Forti L, Conde D, Diez M (2014). Adding ivabradine may reduce elevated heart rate in acute patients when beta blockers are ineffective. *American Journal of Emergency Medicine* **32**: 471–472. DOI 10.1016/j.ajem.2014.01.017.

Wang L, Quan N, Sun W, Chen X, Cates C, Rousselle T, Zhou X, Zhao X, Li J (2018). Cardiomyocyte-specific deletion of Sirt1 gene sensitizes myocardium to ischaemia and reperfusion injury. *Cardiovascular Research* **114**: 805–821. DOI 10.1093/cvr/cvy033.

Xia S, Wang Y, Zhang Y, Deng SB, Du JL, Wang XC, She Q (2010). Dynamic changes in HCN2, HCN4, KCNE1, and KCNE2 expression in ventricular cells from acute myocardial infarction rat hearts. *Biochemical and Biophysical Research Communications* **395**: 330–335. DOI 10.1016/j.bbrc.2010.04.003.

Xiang X, Zhou Y, Sun H, Tan S, Lu Z, Huang L, Wang W (2019). Ivabradine abrogates TNF-α-induced degradation of articular cartilage matrix. *International Immunopharmacology* **66**: 347–353. DOI 10.1016/j.intimp.2018.11.035.

Yamaguchi H, Weil MH, Tang W, Kamohara T, Jin X, Bisera J (2002). Myocardial dysfunction after electrical defibrillation. *Resuscitation* **54**: 289–296. DOI 10.1016/S0300-9572(02)00149-1.

Yang M, Che L, Hua T, Zou Y, Yang Z (2020). Beneficial effects of Ivabradine on post-resuscitation myocardial dysfunction in a porcine model of cardiac arrest. *Shock* **53**: 630–636. DOI 10.1097/SHK.0000000000001403.

Yang M, Hu X, Lu X, Wu X, Xu J, Yang Z, Qian J, Sun S, Cahoon J, Tang W (2015). The effects of α- and β-adrenergic blocking agents on postresuscitation myocardial dysfunction and myocardial tissue injury in a rat model of cardiac arrest. *Translational Research* **165**: 589–598. DOI 10.1016/j.trsl.2014.10.012.

Yip AM, Zhai AB, Haddad H (2016). Heart rate and heart failure. *Current Opinion in Cardiology* **31**: 204–208. DOI 10.1097/HCO.0000000000000266.

Yu HD, Xia S, Zha CQ, Deng SB, Du JL, She Q (2015). Spironolactone regulates hcnprotein expression through micro-RNA-1 in rats with myocardial infarction. *Journal of Cardiovascular Pharmacological* **65**: 587–592. DOI 10.1097/FJC.0000000000000227.

Yu Y, Hu Z, Li B, Wang Z, Chen S (2018). Ivabradine improved left ventricular function and pressure overload-induced cardiomyocyte apoptosis in a transverse aortic constriction mouse model. *Molecular and Cellular Biochemistry* **450**: 25–34. DOI 10.1007/s11010-018-3369-x.

Zhang Q, Li C (2013). Combination of epinephrine with esmolol attenuates post-resuscitation myocardial dysfunction in a porcine model of cardiac arrest. *PLoS One* **8**: e82677. DOI 10.1371/journal.pone.0082677.